Sixth International Symposium on Turbulence and Shear Flow Phenomena
Seoul, Korea, 22-24 June 2009

SIMULATIONS OF HEAT TRANSFER IN A BOUNDARY LAYER SUBJECT TO FREE-STREAM TURBULENCE

Qiang Li, Philipp Schlatter, Dan S. Henningson
Linné FLOW Centre,
KTH Mechanics
Osquars Backe 18, Stockholm, SE-100 44, Sweden
qiang@mech.kth.se

ABSTRACT

The present study investigates the effects of the ambient free-stream turbulence (FST) on the momentum and heat transfer in a turbulent flat-plate boundary layer via large-eddy simulations (LES) using the ADM-RT model. Due to a FST of 20%, the skin-friction coefficient c_f and Stanton number St are substantially elevated up to 15% in the fully turbulent region. The depression of both the mean velocity and temperature profiles in the wake region due to the FST is observed, however, the influence on the wall-normal heat flux in the near-wall region is negligible.

INTRODUCTION

The aim of this study is to perform numerical simulations to investigate the influence of free-stream turbulence (FST) on the momentum and heat transfer in a spatially evolving, fully turbulent boundary layer. Due to the ambient turbulence, such a boundary layer will undergo rapid bypass transition (see *e.g.* Brandt *et al.*, 2004) before reaching a turbulent state. This problem is of interest in many industrial applications in particular related to turbomachinery. Bradshaw (1974) performed the landmark work in this field and later a series of studies have been carried out, *e.g.* Simonich and Bradshaw (1978), Hancock and Bradshaw (1983, 1989). These authors analysed the influence of the grid-generated FST in terms of both turbulence level and turbulent length scale. Up to 30% increase in the Stanton number due to 6% FST is reported. Blair (1983) also reported that the momentum and heat transfer is augmented by grid-generated FST and that the heat transfer seems to be much more affected in a turbulent boundary layer. However, only as much as 20% increase for the heat transfer of a boundary layer under 7% FST was reported. Using the wake of a free jet as the inflow FST, Maciejewski and Moffat (1992) reported a $1.8 \sim 4$ fold absolute augmentation in Stanton number due to free-stream turbulent fluctuations from $20\% \sim 60\%$. The extraordinarily high increase in the Stanton number might, however, be due to the incoming large-scale, anisotropic FST. In spite of the number of studies during the last decades, the problem at hand is still not fully understood. The conclusions from all the studies are general, but the magnitude of the heat transfer enhancement varies considerably from one study to another (Maciejewski and Moffat, 1992).

Therefore, one could resort to numerical simulation. As the modern computers developed during the last 20 years, numerical simulation, in particular direct numerical simulations (DNS) and large-eddy simulations (LES), have become important tools for transition and turbulence research. Péneau *et al.* (2000, 2004) investigated the influence of high levels of FST on a spatially evolving turbulent boundary layer using LES with a dynamic mixed subgrid-scale (SGS) model. Some of the previous experimental observations were reproduced by their simulations. They further reported that the mean temperature profiles exhibit different slopes in the logarithmic region with increasing FST intensity whereas the velocity profiles remain essentially unchanged. Jacobs and Durbin (2000) have performed DNS of bypass transition at lower turbulence intensities including heat transfer ($Pr = 0.71$) and found a generally high correlation between the temperature and (streamwise) velocity during transition. In the turbulent regime, a minor reduction of the temperature profile in both the wake and logarithmic region could be observed.

The aim of the present study is to numerically examine the influence of ambient FST on the momentum and heat transfer at the wall in a fully turbulent boundary layer. Open questions related to quantifying the increase of the friction coefficient and the Stanton number due to high levels of FST shall be addressed. Coupled to these issues is the validity of the Reynolds analogy commonly applied for modelling purposes. As also suggested by Blair (1983), effects of the FST on turbulent heat transfer within the boundary layer are discussed.

NUMERICAL METHODOLOGY

Numerical method and SGS modelling

The filtered three-dimensional, time-dependent, incompressible Navier–Stokes equations are solved using a pseudo-spectral method (Chevalier *et al.*, 2007), *i.e.* Fourier series are employed in the wall-parallel directions and the wall-normal direction is discretised with Chebyshev polynomials. One more equation governing the heat transfer is solved with the same discretisation with the Prandtl number being 0.71. Since there is no feedback force, the temperature field is considered as a passive scalar. No-slip and isothermal wall boundary conditions are employed for velocity and temperature, respectively. The sub-grid scale stress model used is the ADM-RT model (Schlatter *et al.*, 2004) extended to also include passive scalars. Time is advanced with a mixed Runge–Kutta/Crank–Nicolson scheme. At the downstream end of the domain, a "fringe region" is added to fulfil the periodic boundary condition in the streamwise direction. In this region, the outflow is forced by a volume force to the laminar inflow condition, *i.e.* the Blasius boundary-layer profile. In addition, to trigger rapid laminar-turbulent transition, a random volume forcing located at a short distance downstream of the inlet ($x = 10, Re_x = 33400$) is used.

Free-stream turbulence generation

The boundary layer is subject to external disturbances,

i.e. free-stream turbulence which is generated by a superposition of eigenmodes of the Orr-Sommerfeld/Squire operator from the continuous spectrum (Brandt *et al.*, 2004). A similar way is also used by Jacobs and Durbin (2000). The generated FST is designed to be homogeneous and isotropic, following the von Kármán spectrum,

$$E(\kappa) \propto \frac{\kappa^4}{(C+\kappa^2)^{17/6}} \tag{1}$$

with C being a constant and κ denoting the spatial wavenumber. For small wavenumbers κ, *i.e.* large scales, such a spectrum is asymptotically proportional to κ^4, whereas the Kolmogorov $-\frac{5}{3}$ spectrum is recovered for large κ. Following Tennekes and Lumley (1972), an integral length scale L characterising the FST is defined as

$$L = \frac{1.8}{\kappa_{max}} , \tag{2}$$

where κ_{max} is the wavenumber of the maximum energy.

Note that each individual eigenmode of the Orr-Sommerfeld/Squire operator satisfies the continuity constraint, so the disturbances obtained by summing up different modes satisfy continuity as well. These disturbances are then introduced in the fringe region and subsequently advected downstream. Due to the high level of FST at the top boundary, the time step is limited and numerical instabilities might appear. Therefore, all the eigenfunctions are multiplied by a smooth step function above certain hight y_{damp} (non-dimensionalised by the displacement thickness at the inlet δ_0^*). In the present simulations, y_{damp} is chosen to be $y_l - 20$ where y_l is the total height of the computational domain.

Besides the free-stream turbulence in the velocity field, ambient disturbances in the temperature field are generated in a similar fashion as generating the "velocity" turbulence, but based on the continuous spectrum of the linearised temperature equation. The intensities of both the velocity and temperature disturbances can be controlled independently, therefore their influences on transitional and turbulent heat transfer can be examined individually.

The comparisons from different cases are made at the same Reynolds number based on certain measures of the boundary-layer thickness, *e.g.* $Re_\theta = \frac{U_\infty \theta}{\nu}$ or $Re_\tau = \frac{u_\tau \delta_{95}}{\nu}$ where U_∞ is the free-stream velocity, u_τ the friction velocity, θ the momentum thickness and δ_{95} the 95% boundary-layer thickness. By using these Reynolds numbers, the effect of the transition location on the data is removed. Due to the high FST levels, the momentum thickness θ is not appropriate, therefore, another definition θ_{95} defined by only integrating up to the 95% boundary-layer thickness is used in some cases. For the present numerical setup, possible history effects of the FST cannot be considered, *i.e.* the FST effects only depend on the local turbulence intensity and the length scale. To investigate the historical effects of the FST, one has to include the leading edge of the plate.

Simulation parameters

The main parameters defining the problem are the Reynolds number, the intensities of both the velocity free-stream turbulence Tu and the thermal free-stream turbulence T_θ and the corresponding turbulence length scale L. The size of the computational box has to be large enough to accommodate the largest scales of the FST, in particular its width and height which does restrict the admissible inflowing FST modes. Therefore, different computational boxes have been chosen depending on the length scale L of the FST, see Table 1 and 2. The inflow Reynolds number is defined by the displacement thickness of the boundary layer at the inflow boundary of the computational domain (δ_0^*) and was chosen 300 for all cases; thus the laminar inflow is located at $Re_x \approx 30400$. All the quantities are non-dimensionalised with the inlet displacement thickness δ_0^* and the free-stream velocity U_∞.

Table 1: Spatial resolution and box dimensions (including fringe region) for the present simulations.

	$x_l \times y_l \times z_l$ δ_0^*	$N_x \times N_y \times N_z$ (resolution)	$Re_{\delta_0^*}$
Box 1	$1000 \times 60 \times 50$	$256 \times 121 \times 36$	300
Box 2	$1500 \times 90 \times 90$	$384 \times 121 \times 96$	300
Box 3	$1500 \times 180 \times 180$	$384 \times 201 \times 128$	300
Box 4	$750 \times 40 \times 34$	$1024 \times 289 \times 128$	450

Table 2: Parameters used to define the FST and the corresponding computational domain for the simulations. Note that in Case 1, laminar-turbulent transition is only due to the FST whereas in the other cases an additional random forcing close to the inflow , *i.e.* the trip forcing, is active such that a large part of the computational box is turbulent. Case 5 corresponds to the DNS simulation by Li *et al.* (2009).

	Tu %	T_θ %	L δ_0^*	Box
Case 1	4.7	0, 4, 10, 40, 80	5	Box 1
Case 2	0	0	0	Box 2
Case 3	4.7, 20	0	2.5, 5, 7.5	Box 2
Case 4	4.7, 20	0	5, 7.5, 15	Box 3
Case 5	0	0	0	Box 4

RESULTS

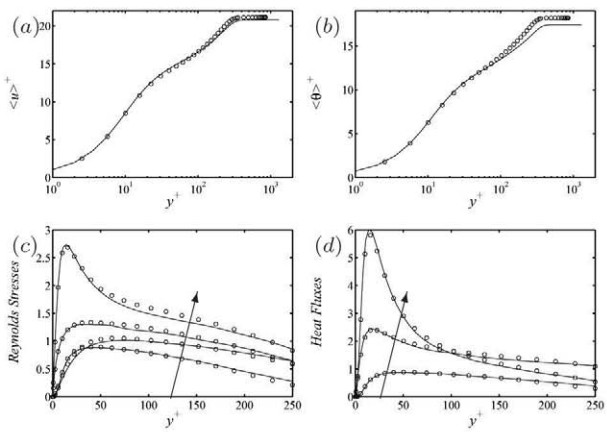

Figure 1: Validation of the LES results (Case 2) at $Re_\theta = 800$. ——— Present LES data, ○ DNS data from Li (2009). (*a*) Mean streamwise velocity, (*b*) Mean temperature, (*c*) Reynolds stresses, the arrow indicates the quantities: $-\langle u'v' \rangle^+$, v^+_{rms}, w^+_{rms}, u^+_{rms}, (*d*) Heat fluxes: $-\langle v'\theta' \rangle^+$, θ^+_{rms}, $\langle u'\theta' \rangle^+$.

Validation of the LES results

The ADM-RT model has been shown to obtain accurate results at a fairly low computational cost in turbulent channel flows by Schlatter *et al.* (2004, 2006). Recently, this model has been extended also to include passive scalar by assuming a constant turbulent Prandtl number Pr_t being 0.6. A comparison with the DNS results obtained by Li *et al.* (2009) at $Re_\theta = 800$ is shown in Figure 1. In general, the results of both the velocity and heat transfer compare reasonably well with the DNS data, especially the turbulence intensities and the heat fluxes are predicted accurately. The larger discrepancies in the mean temperature profile are mainly due to the low resolution used in the streamwise direction. The grid spacing in the streamwise direction Δx^+ (the wall units are calculated based on the friction velocity u_τ at centre of the domain) for the present LES is about 60.

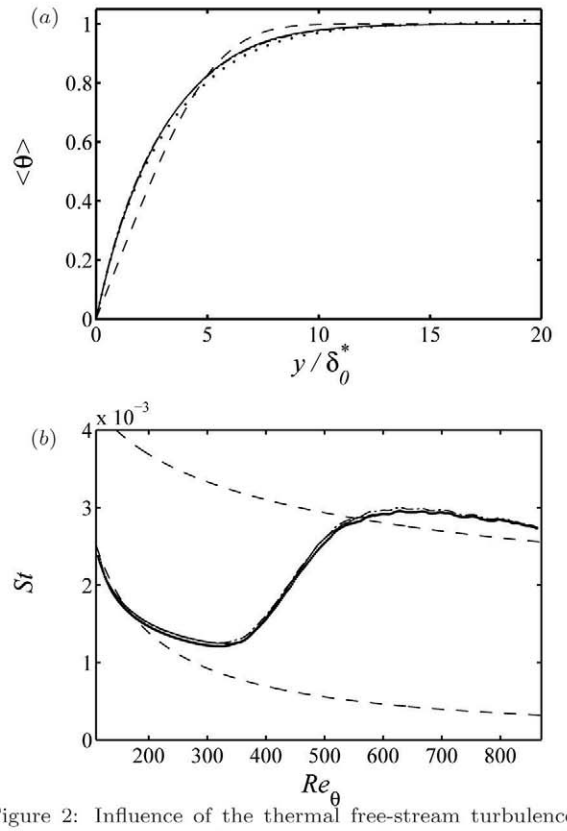

Figure 2: Influence of the thermal free-stream turbulence (Case 1). ——— $T_\theta = 0\%$, –·– $T_\theta = 10\%$, ····· $T_\theta = 80\%$, (a) Mean temperature profile at $Re_\theta = 395$ ($Re_x = 210400$), – – – – laminar temperature profile, (b) Stanton number, – – – – laminar and turbulent correlation.

Influence of the thermal free-stream turbulence T_θ

The influence of the thermal free-stream turbulence $T_\theta = \theta_{rms}$ has been investigated in a smaller computational box (Box 1). In Figure 2, the mean temperature at a fixed downstream position, $Re_x = 210400$ or $Re_\theta = 395$, as well as the evolution of the Stanton number are shown. The laminar temperature profile is also included for comparison. For these cases, the velocity disturbance level is fixed at $Tu = 4.7\%$ while the thermal intensity T_θ is varied from 0% up to 80%. Nevertheless, the changes in the mean profile and the Stanton number are almost negligible. It can therefore be concluded that a higher fluctuation level of the temperature will not lead to an increased heat transfer at the wall. To further confirm these findings, the distributions of the

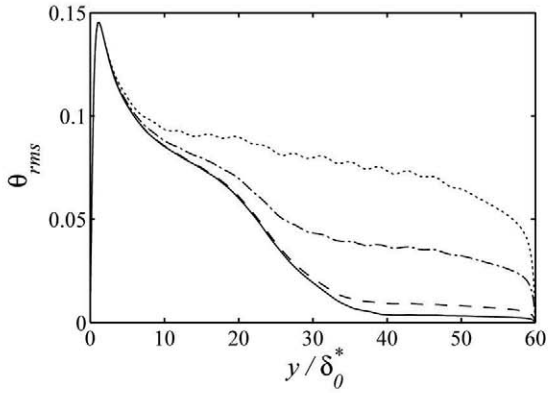

Figure 3: RMS fluctuation of the temperature at $Re_\theta = 790$ ($Re_x = 390400$) (Case 1). ——— $T_\theta = 4\%$, – – – – $T_\theta = 10\%$, –·– $T_\theta = 40\%$, ····· $T_\theta = 80\%$.

temperature fluctuations at $Re_x = 390400$ or $Re_\theta = 790$ are compared in Figure 3. Note that the decay of the fluctuations for $y > 45$ is due to the employed damping function in the free stream. The high levels of temperature fluctuations outside the boundary layer do not influence the growth of the streaky disturbances close to the wall. Consequently the heat transfer at the wall is not increased even for $T_\theta = 80\%$, as shown in Figure 2 (b). Therefore, only Tu will be considered afterwards, and T_θ is set to zero.

Decay of the free-stream turbulence

The FST is well characterised by both the turbulence intensity of the three different velocity components and a

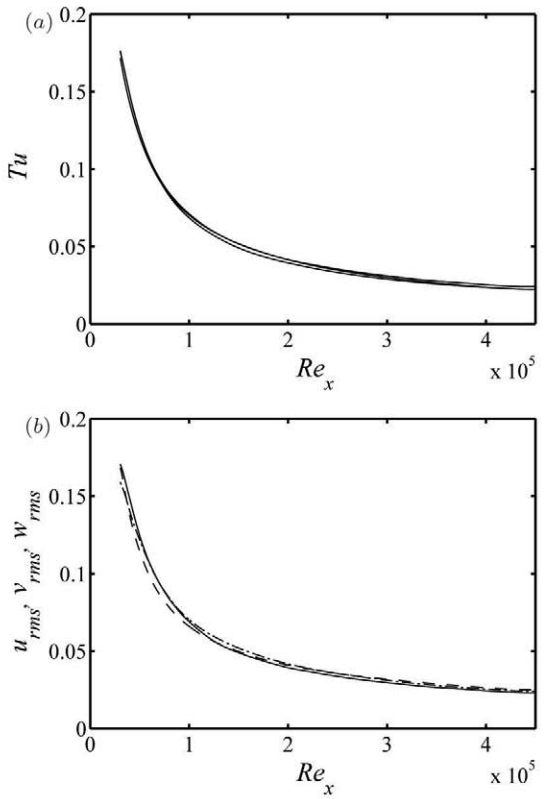

Figure 4: Downstream decay of the FST (Case 4). (a) Turbulence intensity versus the Reynolds number at $y = 50, 100, 150$ with $L = 7.5$, (b) Root-mean-square of the velocity fluctuations versus the Reynolds number at $y = 50$ with $L = 7.5$. ——— u_{rms}, – – – – v_{rms}, –·– w_{rms}.

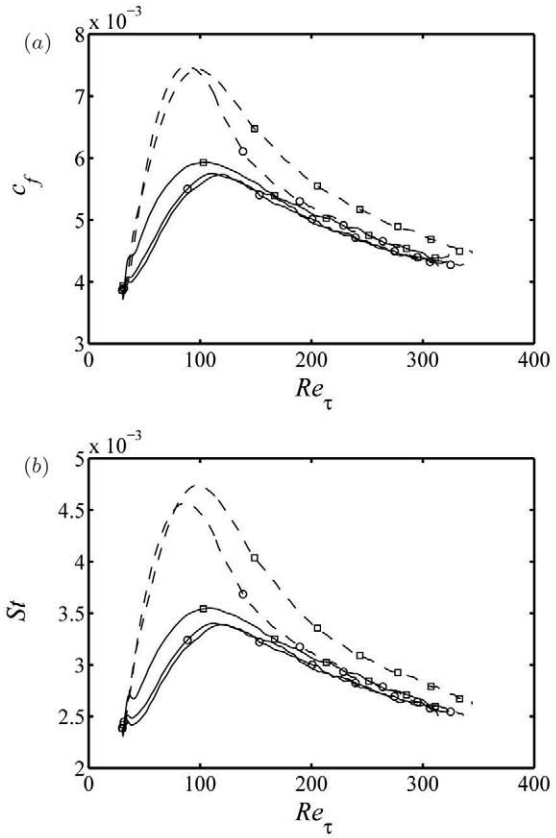

Figure 5: Influence of the turbulence intensity on the skin-friction coefficient c_f and Stanton number St. ——— Case 2, –○–, Case 3 with $Tu = 4.7\%$, $L = 2.5$, –□–, Case 4 with $Tu = 4.7\%$, $L = 7.5$, – –○– –, Case 3 with $Tu = 20\%, L = 2.5$,– –□– –, Case 4 with $Tu = 20\%$, $L = 7.5$, (a) c_f, (b) St.

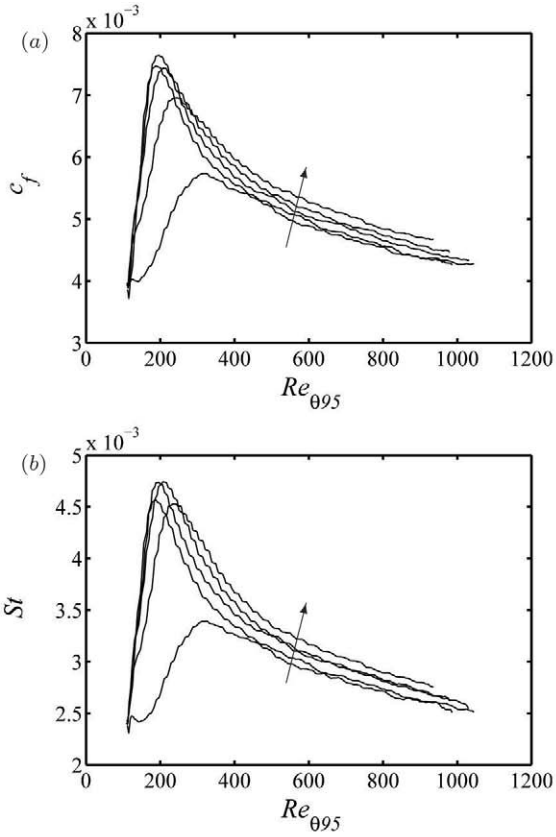

Figure 6: Influence of the length scale on the skin-friction coefficient c_f and Stanton number St with $Tu = 20\%$. The arrow indicates the increasing $L = [0, 2.5, 5, 7.5, 15]$. (a) c_f, (b) St.

measure of the length scale together with energy spectrum. At the inlet, the generated FST is supposed to be nearly isotropic and homogeneous. In particular, the decay rate of the FST is similar to that of the grid turbulence widely used in the experiments. Figure 4 shows the downstream decay of the FST. Tu at different wall-normal positions above the boundary layer and the differences among the velocity intensity components indicate that the homogeneity and the isotropy of the FST are well achieved. It is possible to show that the decay obeys an power law and a more rapid decay of the FST for smaller length scale can be observed (not shown here) which is consistent with the previous results by Brandt *et al.* (2004).

Averaged results

The averaging denoted by the angular brackets $\langle\rangle$ is performed over both the homogeneous spanwise direction and time. The corresponding fluctuating part is denoted by a prime. The influence of the free-stream turbulence level Tu and length scale L on the skin-friction coefficient c_f and the Stanton number St for $Pr = 0.71$ are shown in Figures 5 and 6. The present LES results of the skin-friction coefficient c_f and the Stanton number St from the no FST reference case (Case 2) are about 4% and 7% larger than the DNS results by Li *et al.* (2009). Consistent results for the skin-friction coefficient c_f compared to the previous numerical simulations (*e.g.* Brandt *et al.*, 2004) can be established: For a higher turbulence intensity Tu, a clearly earlier transition to turbulence leading to an increase of c_f can be observed. A similar behaviour also applies to the Stanton number St. Different trends were observed in the simulations by Péneau *et al.* (2000). All the increases in the skin-friction coefficient c_f are about the same for the FST intensities investigated in their simulations from 7% $\sim$ 21%. Due to the small length scale $L = 2.5$, the effects from the FST are much reduced (Hancock and Bradshaw, 1983). The FST decays very rapidly and therefore the distributions of both skin-friction coefficient c_f and the Stanton number St are almost lying on top of the case with no FST in the fully turbulent region. Once the length scale is increased, the FST will decay slower and this will lead to elevation in both c_f and St. For the length scales examined in the present study, the larger the length scale is, the more the skin-friction coefficient and Stanton number will increase. However, the skin-friction coefficient and Stanton number will start decreasing if the length scale is too large compared to the boundary-layer thickness, assuming at a given FST level Tu (Hancock, 1978). The reason for the decreased effects of the FST for increasing length scale is that the no-slip condition of the wall-normal velocity at the wall reduces the intensity of the wall-normal velocity component (Thomas and Hancock, 1977). This effect is not observed in the present simulation due to the comparably small length scales of the generated FST. As noted by Blair (1983), the impact of the length scale of the FST is to reach the maximum at $\frac{L_u}{\delta_{99}} = 1$ with L_u being the streamwise dissipation length scale and δ_{99} being the 99% boundary-layer thickness. For the ratio which is either significantly larger or smaller than unity, the effects would be expected to diminish.

The increases of St compared to Case 2, (*i.e.* no FST

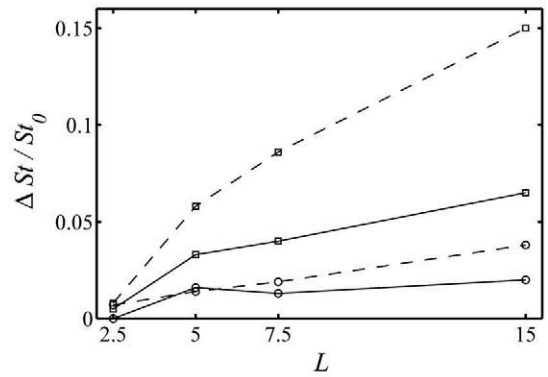

Figure 7: Increase of Stanton number St versus the length scale L. ——— at $Re_{\theta_{95}} = 800$, - - - - at $Re_\tau = 300$, ○ at $Tu = 4.7\%$, □ at $Tu = 20\%$.

reference case, denoted by a suffix "0",) at $Re_{\theta_{95}} = 800$ and $Re_\tau = 300$ are plotted in Figure 7. Similar results are obtained also for c_f (not shown). In general, for both c_f and St when plotted against $Re_{\theta_{95}}$, the increase is less than when plotted against Re_τ. For the present simulations at $Re_\tau = 300$, a maximum of 15% for St at the turbulence intensity of 20% is achieved. However, Simonich and Bradshaw (1978) reported that at a nominal turbulence intensity of 7% in the fully turbulent region, 10% increase for c_f and 30% for St was observed. At essentially the same turbulence intensity, Blair (1983) reported that both c_f and St increase as much as 20% in the fully turbulent region. In the simulations by Péneau *et al.* (2000), an increase of 10% in c_f and 20% in St are obtained at a turbulence intensity of 21% at $Re_\theta \approx 1100$. At $Re_\theta = 800$, Jacbos and Durbin (2000) obtained about 5% increase in c_f and 12% in St with turbulence intensity around 4%. The considerably larger increase in St than in c_f observed in the experiments by Simonich and Bradshaw (1978) and the mentioned other simulations are not confirmed in the present simulations. This might be due to the present employed LES model and the low resolution used for the simulations. However, as pointed out in Maciejewski and Moffat (1992), the larger effects observed by Simonich and Bradshaw (1978) are possiblely due to the change in the transition location on the flat plate. The FST for the present simulation decays fast compared to the experiments due to relatively small length scales. The local FST level at $Re_{\theta_{95}}$ or $Re_\tau = 300$ is less than 3% (see Figure 4). Taking this into account, 15% increases of both c_f and St for a local $Tu = 3\%$ are comparable to the experiments.

The mean velocity and temperature profiles from Case 4 showing the influences of the FST are plotted in Figure 8. All of the profiles are taken at $Re_{\theta_{95}} = 800$. The log-law is also included for comparison. It is clearly seen that the profiles in the logarithmic region are insensitive to the FST whereas in the wake region significant depression of the boundary-layer wake starts appearing. Especially for the case of $Tu = 20\%$, the wake region even vanishes. For the temperature profiles, a similar conclusion can be drawn, *i.e.* only the wake region is influenced by the FST while the viscous sub-layer and logarithmic region are unchanged. These results are consistent with the previous experimental work by Blair (1983). However, Maciejewski and Moffat (1992) reported that only for the temperature profile, the depression extends even below the wake region down to the logarithmic region. The results by Péneau *et al.* (2000) show that the slope of the logarithmic region varies significantly with Tu for the temperature profile, which can not be confirmed

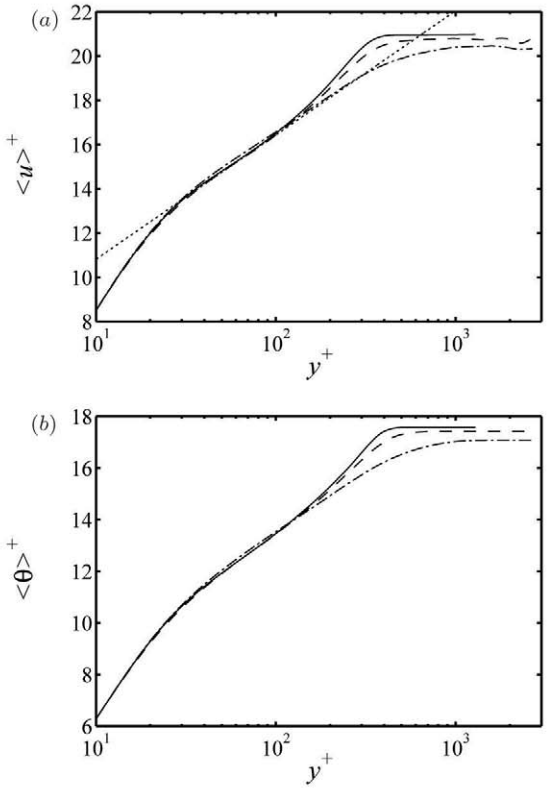

Figure 8: Influence of the FST on the mean profiles of velocity and temperature at $Re_{\theta_{95}} = 800$. ——— Case 2, - - - - Case 4 with $Tu = 4.7\%$, $L = 15$, —·— Case 4 with $Tu = 20\%$, $L = 15$, ····· $\langle u \rangle^+ = \frac{1}{0.41} \ln y^+ + 5.2$. (*a*) $\langle u \rangle^+$, (*b*) $\langle \theta \rangle^+$.

here.

The RMS fluctuation of the streamwise velocity for different turbulence intensities together with the DNS data from Li *et al.* (2009) are shown in Figure 9 (*a*). A slight increase of the peak value and a decrease of the peak position from the wall for the u_{rms} are observed. The relatively large increase far away from the wall, *i.e.* $y^+ > 200$, due to the FST is also noticeable. A similar behaviour also exists for the temperature fluctuations. On the contrary, the shear stress $\langle u'v' \rangle^+$ (not shown here) and the wall-normal heat flux $\langle v'\theta' \rangle^+$ remain unchanged except in the outer part of the boundary layer. The reason for the unaltered profiles of $\langle u'v' \rangle^+$ and $\langle v'\theta' \rangle^+$ in the near-wall region might be that the perturbations enter the boundary layer mainly in the streamwise velocity component (Brandt *et al.*, 2004). However, Péneau *et al.* (2000) observed a different trend: The peak values of $\langle u'v' \rangle^+$ and $\langle v'\theta' \rangle^+$ are increased considerably in both the logarithmic and wake region and the peak positions are displaced noticeably towards the wake.

CONCLUSIONS AND OUTLOOK

Simulations of turbulent boundary-layer flow with heat transfer under the influence of free-stream turbulence have been performed. Since the behaviour of the velocity disturbances inside and outside the boundary layer for a transitional case is well understood (see *e.g.* Brandt *et al.*, 2004), the focus of the present contribution is to examine the influences of the ambient turbulence on momentum and heat transfer in a fully turbulent flow; in particular whether an increased Stanton number can be observed for high turbulence intensities.

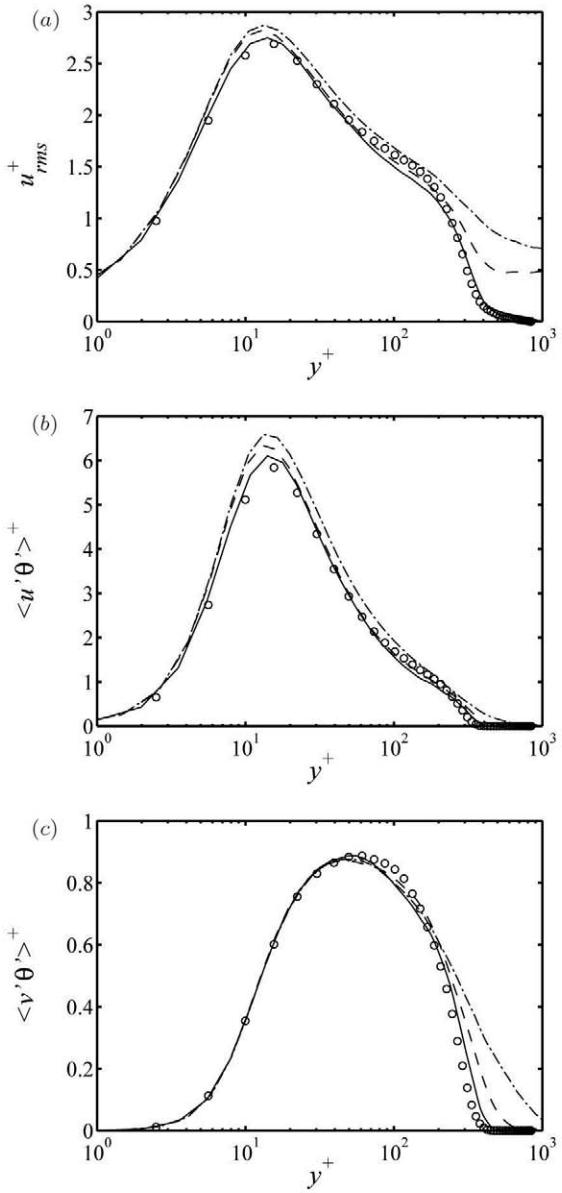

Figure 9: Influence of the FST on the turbulent intensity, heat fluxes and turbulent Prandtl number at $Re_{\theta_{95}} = 800$. ——— Case 2, - - - - Case 4 with $Tu = 4.7\%$, $L = 15$, —·— Case 4 with $Tu = 20\%$, $L = 15$, ∘ DNS data from Li *et al.* (2009). (*a*) u^+_{rms}, (*b*) $\langle u'\theta' \rangle^+$, (*c*) $\langle v'\theta' \rangle^+$.

A detailed parameter study varying both the turbulence intensity and the length scale of the velocity has been conducted. In particular, the simulation domains are chosen large enough such that the relevant part of turbulent boundary-layer flow can be included in the computational domain. The results obtained are consistent with previous observations. The LES results with no FST are validated against the DNS results and the agreement in general is reasonably good.

The mean velocity and temperature profiles are unaffected by the FST in the viscous sub-layer and the logarithmic region. On the other hand, more depression of the wake region can be observed with increasing turbulence intensity. Both the skin-friction coefficient and the Stanton number increase with increasing free-stream turbulence intensity (as much as 15% for a nominal turbulence intensity of 20% at the inlet). Taking into account the low local turbulence intensity, the increase is on the same level as observed in the experiments. In the future, to validate the heat-transfer results with FST, a series of direct numerical simulations shall be carried out to ensure the accuracy of the current LES predictions.

REFERENCES

Blair, M. F., 1983, "Influence of free-stream turbulence on turbulent boundary layer heat transfer and mean profile development, Part I and II," *ASME J. Heat Transfer*, Vol. 105, pp. 33-47.

Bradshaw, P., 1974, "Effect of free-stream turbulence on turbulent shear layers," I.C., *Aero Report 74-10*, Imperial College of Science and Technology, Department of Aeronautics, Prince Consort Road, London SW7 2BY.

Brandt, L., Schlatter, P., and Henningson, D. S., 2004, "Transition in boundary layers subject to free-stream turbulence," *J. Fluid Mech.*, Vol. 517, pp. 167-198.

Chevalier, M., Schlatter, P., Lundbladh, A. and Henningson, D. S., 2007, "SIMSON A pseudo-spectral solver for incompressible boundary layer flows," *Technical Report TRITA-MEK 2007:07*, KTH Mechanics, Stockholm, Sweden.

Hancock, P. E. 1978, *Effect of free-stream turbulence on turbulent boundary layers*, PhD Thesis, Imperial College of Science and Technology, University of London.

Hancock, P. E., and Bradshaw, P., 1983 "The effect of free-stream turbulence on turbulent boundary layers," *ASME J. Fluids Eng.*, Vol. 105, pp. 284-289.

Hancock, P. E., and Bradshaw, P., 1989, "Turbulence structure of a boundary layer beneath a turbulent free stream," *J. Fluid Mech.*, Vol. 205, pp. 45-76.

Jacobs, R. G., and Durbin, P. A., 2000, "Bypass transition phenomena studied by computer simulation," *Tech. Rep. TF-77*, Flow Physics and Computation Division, Department of Mechanical Engineering, Stanford Univ., CA.

Li, Q., Schlatter, P., Brandt, L. and Henningson, D. S., 2009, "Direct numerical simulation of a turbulent boundary layer with passive scalar transport," *Direct and Large-Eddy Simulation VII*, Springer-Verlag, Berlin. To appear.

Maciejewski, P. K. and Moffat, R. J., 1992, "Heat transfer with very high free-stream turbulence: Part I and II," *ASME J. Heat Transfer*, Vol. 114, pp. 827-839.

Péneau, F. and Boisson, H. C. and Djilali, D., 2000, "LES of the influence of high free-stream turbulence on a spatially evolving boundary layer," *Int. J. Heat Fluid Flow*, Vol. 21 (5), pp. 640-647.

Péneau, F. and Boisson, H. C. and Kondjoyan, A. and Djilali, D., 2004, "Structure of a flat plate boundary layer subjected to free-stream turbulence," *Int. J. Comput. Fluid Dynamics*, Vol. 18 (2), pp. 175-188.

Schlatter, P., Stolz, S. and Kleiser, L., 2004, "LES of transitional flows using the approximate deconvolution model," *Int. J. Heat Fluid Flow*, Vol. 25 (3), pp. 549-558.

Schlatter P., Stolz, S. and Kleiser L., 2006, "LES of spatial transition in plane channel flow," *J. Turbulence*, Vol. 7 (33), pp. 1-24.

Simonich, J. C. and Bradshaw, P., 1978, "Effect of free-stream turbulence on heat transfer through a turbulent boundary layer," *J. Heat Transfer*, Vol. 100, pp. 671-677.

Tennekes, H. and Lumley, J. L., 1972, *A First Course in Turbulence*, The MIT Press, Cambridge, M.A.

Thomas, N. H. and Hancock, P. E., 1977, "Grid turbulence near a moving wall," *J. Fluid Mech.*, Vol. 82, pp. 481-496.